JACS
JOURNAL OF THE AMERICAN CHEMICAL SOCIETY
Article
pubs.acs.org/JACS

Electronic Excited States Responsible for Dimer Formation upon UV Absorption Directly by Thymine Strands: Joint Experimental and Theoretical Study

Akos Banyasz,[†] Thierry Douki,[‡] Roberto Improta,*[,§] Thomas Gustavsson,[†] Delphine Onidas,[†,⊥] Ignacio Vayá,[†] Marion Perron,[†] and Dimitra Markovitsi*[,†]

[†]CNRS, IRAMIS, SPAM, Laboratoire Francis Perrin, URA 2453, 91191 Gif-sur-Yvette, France

[‡]CEA, INAC, SCIB, UJF & CNRS, LCIB (UMR_E 3 CEA-UJF and FRE 3200), Laboratoire "Lésions des Acides Nucléiques", 17 Rue des Martyrs, F-38054 Grenoble Cedex 9, France

[§]Istituto Biostrutture e Bioimmagini-CNR, Via Mezzocannone 16, I-80134 Napoli, Italy

Supporting Information

ABSTRACT: The study addresses interconnected issues related to two major types of cycloadditions between adjacent thymines in DNA leading to cyclobutane dimers (T<>Ts) and (6-4) adducts. Experimental results are obtained for the single strand $(dT)_{20}$ by steady-state and time-resolved optical spectroscopy, as well as by HPLC coupled to mass spectrometry. Calculations are carried out for the dinucleoside monophosphate in water using the TD-M052X method and including the polarizable continuum model; the reliability of TD-M052X is checked against CASPT2 calculations regarding the behavior of two stacked thymines in the gas phase. It is shown that irradiation at the main absorption band leads to cyclobutane dimers (T<>Ts) and (6-4) adducts via different electronic excited states. T<>Ts are formed via $^1\pi\pi^*$ excitons; [2 + 2] dimerization proceeds along a barrierless path, in line with the constant quantum yield (0.05) with the irradiation wavelength, the contribution of the $^3\pi\pi^*$ state to this reaction being less than 10%. The formation of oxetane, the reaction intermediate leading to (6-4) adducts, occurs via charge transfer excited states involving two stacked thymines, whose fingerprint is detected in the fluorescence spectra; it involves an energy barrier explaining the important decrease in the quantum yield of (6-4) adducts with the irradiation wavelength.

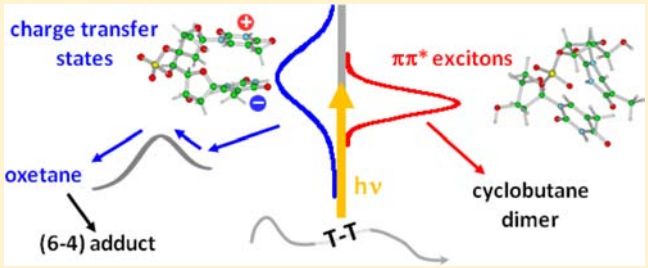

INTRODUCTION

Cyclobutane thymine dimers (T<>Ts) and (6-4) adducts (Figure 1) are major mutagenic photoproducts formed upon absorption of UV irradiation directly by DNA.[1] A large number of articles, appeared since the 1960s, discussed their formation mostly in terms of generic "singlet" or "triplet" excited states.[1] According to these studies, the reaction leading to (6-4) adducts proceeds exclusively via excited singlet states because these photoproducts cannot be obtained in DNA helices by triplet sensitization. In contrast, both the singlet and the triplet routes are possible in the case of T<>Ts.[1,2]

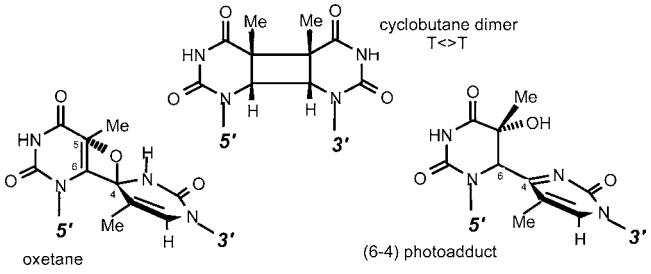

Figure 1. Structure of the two studied thymine dimeric photoproducts and the oxetane intermediate.

During the past decade, a series of experimental and theoretical studies revealed a more complex picture of the DNA excited states and their relaxation.[3−8] In particular, it was shown that the electronic coupling gives rise to delocalized $^1\pi\pi^*$ excited states (excitons) and charge transfer (CT) excited states, which could play a key role in reactivity.[3,4,6,7]

As many of the early works, recent studies, using time-resolved spectroscopic techniques, were carried on thymine oligonucleotides.[9−11] Femtosecond experiments showed that T<>T formation in thymine single strands is an ultrafast process, corroborating their formation in the $^1\pi\pi^*$ singlet state.[10] In parallel, quantum mechanical calculations demonstrated that a barrierless concerted [2 + 2] cycloaddition reaction can indeed proceed on a singlet excited state, which leads to an S_0/S_1 conical intersection (CI).[12] The low T<>T quantum yield ($\phi_{T<>T}$), of the order of 10^{-2}, was attributed to

Received: April 27, 2012
Published: August 15, 2012

   dx.doi.org/10.1021/ja304069f | J. Am. Chem. Soc. 2012, 134, 14834−14845

the control of the reaction by the ground-state conformation.[13,14] The idea that T<>T formation occurs predominantly via $^1\pi\pi^*$ singlet state has been strongly challenged by another time-resolved study which pointed out the role played by the $^3\pi\pi^*$ state.[11] The reactivity of the triplet state toward T<>Ts has also been the subject of theoretical studies.[15]

The formation of (6-4) adducts has been investigated less thoroughly. Nanosecond flash photolysis experiments revealed that they are formed on the millisecond time scale via a reaction intermediate which does not absorb in the 300−700 nm spectral domain.[9] The oxetane (Figure 1), produced by a Paterno−Büchi reaction, was predicted to be a precursor of the (6-4) adducts; being less conjugated than the final photoproduct, it can indeed correspond to this intermediate.[16] Evidence for the involvement of such an intermediate is strongly supported by its isolation in the case of thiothymine.[17] Molecular dynamics simulations suggested that, as in the case of T<>Ts, oxetane formation is also governed by the ground-state conformation; in both reactions a critical distance between the reactive bonds of the two thymines was deduced from comparison with the experimentally determined quantum yields, obtained for a unique irradiation wavelength.[14]

Early studies reported that the quantum yields of the dimerization reactions vary with the irradiation wavelength, but the values published by different groups are not consistent enough to establish a correlation regarding the involved excited states.[18−20] However, all the studies agree that the quantum yield of T<>Ts is considerably higher than that of (6-4) adducts ($\phi_{6\text{-}4}$). Actually, a quantum chemistry study invokes the possibility that oxetane formation proceeds via the $^3\pi\pi^*$ state[21] whereas another theoretical study suggests that it is due to CT states, which are located at much higher energy than the $^1\pi\pi^*$ states.[12] A recent experimental work suggested that CT states are responsible for the weak tail characterizing the absorption spectrum of thymine single strands located in the UVA spectral domain; however, UVA irradiation induces T<>Ts but not (6-4) adducts.[22]

From the above rapid survey, it is clear that, despite the precious information accumulated, there are still important discrepancies regarding the excited states involved in each type of dimerization reaction. Part of them arises from the fact that recent studies, performed with state-of-art techniques, sometimes also base their conclusions on less precise data from older studies. For example, very accurate results obtained by femtosecond broadband fluorescence and absorption spectroscopy are discussed using molar absorption coefficients, fluorescence spectra, intersystem crossing quantum yields, or quantum yields for dimerization reactions, obtained over several decades by various groups under different experimental conditions.[11] Another possible source of confusion is related to theoretical studies. All the quantum chemistry calculations mentioned previously were performed for two stacked thymines in the gas phase.[12,15,21] However, the presence of the charged backbone, water molecules, and counterions may modify greatly both the energetic ordering of the various types of excited states and possible reaction barriers.

With the above questions in mind, we have undertaken a joint experimental and theoretical investigation dealing with the electronic excited states responsible for thymine dimerization in thymine strands. Experiments were performed mainly for the eicosamer $(dT)_{20}$; a few control tests were carried out for the dinucleoside monophosphate TpT, whose quantum yields of dimerization are known to be lower compared to those of long oligonucleotides.[18] The photophysical properties of $(dT)_{20}$, determined by steady-state and time-resolved optical spectroscopy, i.e., fluorescence upconversion (FU), time-correlated single photon counting (TCSPC), and nanosecond flash photolysis, are compared to those of the thymidine monophosphate (TMP). The quantum yields for the formation of T<>Ts and (6-4) adducts are determined for a series of irradiation wavelengths; the photoproducts are monitored by high performance liquid chromatography coupled to mass spectrometry (HPLC/MS). In parallel, the TMP triplet is studied for different excitation wavelengths. Such systematic study, associated with specific experimental protocols, allows us to minimize the experimental artifacts, such as detecting emission from photoproducts or inducing structural changes in the oligomers due to local heating by laser pulses,[23] and to reveal meaningful trends. This is particularly important when photoreactions are related to rare events and very small signals have to be detected.

Calculations are carried out for TpT in water, also considering the counterion (Na^+). We use the time-dependent (TD) DFT method, adopting the M052X functional and including the solvent effect by the polarizable continuum model (PCM). In a first step, we check that the TD-M052X method provides extremely similar description of thymine dimerization in the gas phase with CASPT2 calculations. Subsequently, we present a detailed analysis of the main photochemical reactive paths leading to T<>T and to the oxetane intermediate. These computational results are part of a thorough study of conformational effects on the excited-state behavior of TpT in water, described in a forthcoming theoretical work.[24]

Our joint study provides new insights on the most significant effects modulating the photochemical reactivity of thymine-rich oligonucleotides, indicating that T<>T and (6-4) UV-induced lesions originate from two distinct excited electronic states. In contrast to the barrierless T<>T formation via $^1\pi\pi^*$ excitons, the reaction leading to (6-4) adducts indeed involves an excited CT state and requires important activation energy.

EXPERIMENTAL DETAILS

Materials. The $(dT)_{20}$ strands were purchased from two different suppliers, Eurogentec Europe and Alpha DNA. Several batches from each supplier were tested. They were purified in two different ways using either reverse-phase HPLC or polyacrylamide gel electrophoresis. In addition to the oligomer, we also found that polymeric strands obtained from a third supplier (Amersham Biosciences) give the same qualitative results as that of $(dT)_{20}$. TpT and TMP were purchased from Sigma Aldrich. Thymine strands were dissolved in phosphate buffer (0.1 M NaH_2PO_4, 0.1 M Na_2HPO_4, 0.25 M NaCl) prepared using Millipore water (Milli-Q Synthesis).

The concentration of oligonucleotide solutions was determined as follows. First, oligomers were hydrolyzed into monomeric nucleosides by incubation with phosphodiesterases I and II and alkaline phosphate. Then, the samples were injected on a HPLC system connected to a reverse phase column. Quantification of the nucleoside content was achieved by UV detection, after calibration of the system with authentic standards.

Steady-State Measurements. Steady-state absorption and fluorescence spectra were recorded with a Perkin Lambda 900 spectrophotometer and a SPEX (Fluorolog-3, Jobin-Yvon) spectrofluorimeter, respectively. Emission spectra were recorded at a right-angle configuration and were corrected for the response of the detection system.[25] The fluorescence quantum yields were determined using as a reference either TMP[26] (UVC) or quinine sulfate dihydrate in 0.1 M $HClO_4$[25] (UVA).

The SPEX spectrofluorimeter was also used for continuous irradiations. The monochromator bandwidth was 5 nm. To avoid the formation of a high local concentration of photoproducts, solutions, contained in 10 × 10 mm cells, were gently stirred. During the irradiation, the temperature was kept at 23 ± 0.1 °C by a Huber CC3 apparatus. To determine the number of absorbed photons, the intensity of the exciting beam was continuously monitored by a photodetector which was calibrated before and after the experiment by two different power meters: Melles Griot 13PEM001 and a NIST traceable OPHIR/PD300-UV. The reliability of this method was checked using 1,3-dimethyluracil actinometry.[13,27]

Time-Resolved Fluorescence Experiments. Time-resolved fluorescence experiments were carried out by fluorescence upconversion (FU) and time-correlated single photon counting (TCSPC), using as excitation source the third harmonic (267 nm, 120 fs) of a Ti-sapphire laser (Coherent MIRA 900). The FU setup is described in detail elsewhere.[28] The TCSPC setup used a Becker & Hickl GmbH PC card and microchannel plate (R1564 U Hamamatsu); a Glan-Thomson prism was positioned at the magic angle on the emission side. The instrumental response function was ca. 330 fs and 70 ps, for FU and TCSPC experiments, respectively. To determine the fluorescence anisotropy by FU, temporal scans were made for parallel and perpendicular excitation/detection configurations by controlling the polarization of the exciting beam with a half-wave plate and detecting the vertical component of the fluorescence.

Special cautions were taken to eliminate the contribution of photoproducts to the fluorescence decays. For FU (peak intensity: 0.2 $GWcm^{-2}$), 25 mL of solution was circulated through a flow cell whereas for TCSPC (peak intensity: 3 $kWcm^{-2}$), ca. 3 mL of solution contained in 10 ×10 mm quartz cells was continuously stirred. Successive measurements gave identical decays which were eventually merged to increase the signal-to-noise ratio.

Nanosecond Flash Photolysis. All measurements were carried out for argon-purged solutions at room temperature contained in a 10 × 10 mm quartz cell and continuously stirred. The excitation source was the second harmonic of an optical parametric oscillator (VersaScan GWU), pumped by a Nd:YAG laser (Spectra Physics, 8 ns) and functioning at a repetition rate of 1 Hz. The pulse energy at the surface of the cell varied from 0.5 to 2 mJ. The analyzing beam was provided by a 150 W Xe-lamp (Applied Photophysics); it was dispersed in a SPEX 270 M monochromator, detected by a Hamamatsu R3896 photomultiplier and analyzed by a LeCroy WaveRunner 6050 oscilloscope. The exciting pulse energy was measured by two different detectors: a pyroelectric sensor (OPHIR Nova2, PE25) and an energy ratiometer (Laser precision Instruments, Rj 7200).

Quantification of the Photoproducts. The $(dT)_{20}$ was enzymatically hydrolyzed to release unmodified bases as nucleosides and photoproducts as dinucleoside monophosphates. Two 2-h incubation periods were performed at 37 °C, first with phosphodiesterase II, DNase II, and nuclease P1 (pH 6), and then with phosphodiesterase I and alkaline phosphatase (pH 8). The obtained solutions were analyzed by HPLC/MS using negative electrospray ionization. Selective quantification of the thymine dimeric photoproducts was achieved by multiple reaction monitoring.[29] In this detection mode, the first quadrupole of the mass spectrometer is set at the m/z value of the targeted pseudomolecular ion (i.e., m/z = 545 for thymidine photoproducts released from oligonucleotides as dinucleoside monophosphates). Subsequently, these ions are directed into the second quadrupole, where they are fragmented by collision with molecular nitrogen. The resulting fragments are then directed into the third quadrupole that is set at m/z values specific for the targeted compounds (i.e., m/z = 447 for TpT cyclobutane dimers and m/z = 432 TpT (6-4) photoproduct). Detection of the monitored ions at two stages of selection provides high specificity and sensitivity. For T<>Ts, both the cis,syn and trans,syn diastereoisomers were quantified. Formation of the latter minor photoproduct is possible in single-stranded DNA due to its more flexible structure compared to double-stranded DNA. The linearity of the dimer formation with the number of absorbed photons was verified to rule out occurrence of secondary photoreactions such as photoreversion of T<>Ts or conversion of (6-4) adducts into their Dewar valence isomers. An example is shown in Figure 2.

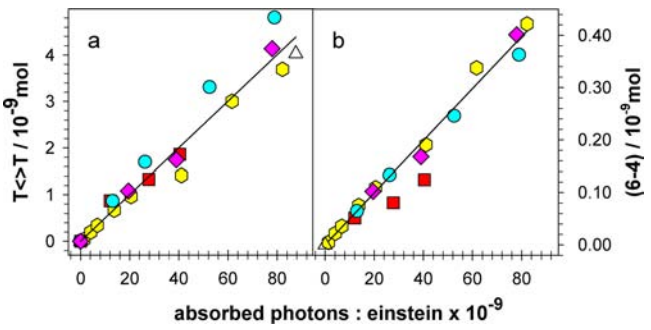

Figure 2. Cyclobutane dimer (a) and (6-4) adduct (b) formation in $(dT)_{20}$ as a function of the photons absorbed at 267 nm. Different symbols correspond to measurements with different batches.

COMPUTATIONAL DETAILS

Density Functional. Most of our analyses were performed by using a recently developed M052X functional,[30,31] based on simultaneously optimized exchange and correlation contributions both including kinetic energy density. This allows a more reliable treatment of dispersion interactions (and therefore a very accurate description of stacked systems) and charge transfer transitions than that were provided by previous density functionals.[6,30,32,33] In some cases, the M052X analysis was complemented with the results obtained by PBE0 functional,[34] allowing a less cumbersome optimization of the CT excited-state minima. Calculations on TpT concern the singly negatively charged species (TpT^-) and that containing the Na^+ counterion (TpTNa).

Solvent Effect. Bulk solvent effects were included by the polarizable continuum model (PCM).[35] Excited-state geometry optimizations in solution have been performed by the "standard" linear-response (LR) implementation of PCM/TD-DFT,[36] for which analytical gradients are available.[37] The results of LR-PCM/TD-DFT geometry optimizations were refined by single-point state-specific (SS) PCM/TD-DFT calculations.[38] In SS approaches, a fully variational formulation of the solvent effect on the excited-state properties is achieved, by solving a different effective Schrödinger equation for each state of interest and thus providing a more balanced description of solvent effects on different excited electronic states compared with that for LR-PCM; this is especially important for CT transitions involving large changes of the electron density.[38,39]

When discussing solvent effects on optical spectra, it is useful to define two limiting situations, usually referred to as nonequilibrium (neq) and equilibrium (eq) time regimes.[35] In the former case, only solvent electronic polarization (fast solvent degrees of freedom) is in equilibrium with the excited-state electronic density of the solute, whereas nuclear degrees of freedom (slow solvent degrees of freedom) are equilibrated with the ground-state electron density. On the contrary, the equilibrium regime is reached when both fast and slow degrees of freedom are equilibrated with the excited-state electron density. In the frame of the PCM formalism, the solvent reaction field in the "neq" regime depends on the dielectric constant at optical frequency ε_{opt}, computed as the square of the solvent refractive index n, ($\varepsilon_{opt} = n^2$, for water 1.776). PCM

dx.doi.org/10.1021/ja304069f | J. Am. Chem. Soc. 2012, 134, 14834−14845

equilibrium solvation is instead ruled by the static dielectric constant (ε, for water 78.39). To calculate absorption spectra and to discuss the fast part of the excited-state dynamics (<200 fs), "neq" solvation energies are more suitable, while the "eq" time regime can better model the excited-state energies for the slower part of the excited-state dynamics and fluorescence process.

Treating solvent effects in the proximity of a CI is not trivial. As a matter of fact, dynamical solvation effects should be explicitly included in the calculations when locating the CI and discussing the excited-state decay by approaches such as those reported in ref 40. However, as already stated, a fully dynamical treatment in the proximity of the CI is outside the scope of this study. Within the present context, "neq" and "eq" PCM calculations can be considered two limiting situations providing a qualitative understanding of the solvent effect. Therefore, we checked that the position and the general features of the S_0/S_1 crossing regions are not affected by the time regime used in PCM calculations (see Supporting Information).

Inhomogeneous broadening was evaluated by a recently developed procedure[41] based on simple but physically well sounded relationships devised by Marcus[42] that have been widely employed in the literature to estimate and analyze the effect of inhomogeneous broadening on absorption spectra. According to our approach, the inhomogeneous broadening is estimated by the solvent reorganization energy calculated by the SS-PCM/TD-DFT method.[41] When it is applied to electronic transitions involving significant change in the electron density, the resulting inhomogeneous broadening differs from experimental values less than 200 cm^{-1}.[41]

Ground- and excited-state geometry optimizations were performed at the PCM/M052X/6-31G(d) level, checking the effect of basis set extension by single point calculations at the 6-31+G(d,p) level. All the calculations were performed with the Gaussian09 program.[44]

Our computational approach has been already successfully applied to the study of oligonucleotide excited states:[6,32,33,45] M052X provides a reliable description of excited-state properties of stacked systems including CT transitions and PCM, despite the absence of explicit solvent molecules, an accurate evaluation of solvent effects.

The use of TD-M052X for studying photochemical paths requires additional considerations. As a matter of fact, TD-DFT calculations are not expected to provide an accurate description of a system in the proximity of a conical intersection. TD-DFT is defined for a nondegenerate ground state, and it has been shown that the dimensionality of the degenerate space around the conical intersection is not correct: it is N-1 (N being the number of internal degrees of freedom of the system under study) instead of N-2.[46] Furthermore, calculations on model systems indicate that the shape of the two potential energy surfaces (PES) around the CI is too steep when compared with multiconfigurational (MC) treatment.[46] On the other hand, several studies show that TD-DFT can provide a fairly reliable estimate of the geometry and the energy of minimum energy CI, especially when double excitations do not play a significant role in the process under investigation.[43,47] The present study is not aimed to provide a detailed quantum dynamical treatment of the photodimerization process (a task that would be, in any case, out of reach for a dinucleotide in solution) but only qualitative insights into the possible reactive paths. No attempt was made to locate the CI by TD-M052X calculations; we simply analyzed the general features of the crossing region with S_0 where excited-state geometry optimizations converge. The very good comparison of the results found for thymine dimer in the gas phase by accurate MC-SCF calculations with those obtained by TD-M052X calculations indicate that the latter method is satisfactory for the purposes of the present study. However, other approaches, such as the MM/MSCASPT2 dynamical calculations, reported in ref 48, should be used when looking for a more direct comparison with the experimental results.

EXPERIMENTAL RESULTS

The steady-state absorption spectrum of $(dT)_{20}$ from the UVC to the UVA spectral domain, as well as its fluorescence spectra with UVC and UVA excitation, is reported in ref 22. In the present study we performed more refined measurements, allowing their detailed comparison with the TMP spectra to reveal cooperative effects.

When going from the monomer to the oligomer, the absorption spectrum exhibits three small, albeit detectable, changes. First, the peak is blue-shifted, from 267.3 to 265.4 nm. Second, the maximum molar absorption coefficient decreases from 9500 to 8900 M^{-1} cm^{-1}. Finally, a weak tail appears at the UVA spectral domain.[22]

The fluorescence spectrum of $(dT)_{20}$, recorded upon excitation at the main absorption band, closely resembles that of TMP, both peaking at 330 nm (Figure 3a). This band is

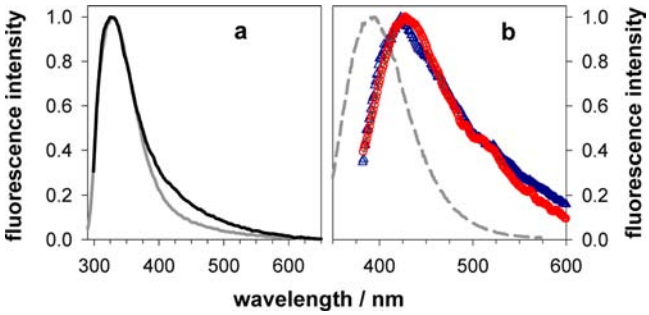

Figure 3. Normalized fluorescence spectra of $(dT)_{20}$ (black) and TMP (gray) obtained following excitation at 255 nm (a). Their difference (blue) is shown in plot b together with the spectrum of $(dT)_{20}$ obtained following excitation at 330 nm (red from reference[22]). In dashes: fluorescence spectrum of (6-4) adducts (λ_{ex} = 325 nm) obtained after prolonged irradiation of $(dT)_{20}$.

correlated with emission from $^1\pi\pi^*$ states.[49] However, the red wing of the polynucleotide spectrum is more intense compared to that of the monomeric chromophore. Subtraction of the two spectra reveals a band peaking at 425 ± 5 nm, whose shape and position coincide with the UVA-induced fluorescence[22] (Figure 3b). If the necessary precautions are not taken (see Experimental Details), this band is blurred by emission from (6-4) adducts, accumulated during the recording of the spectrum and emitting at 393 nm (Figure 3b) with a quantum yield of 0.03.[50]

The energy difference between the peaks of the high and low emission bands of $(dT)_{20}$, determined after conversion of the spectra in energy scale, is 0.85 ± 0.04 eV. Their quantum yields are 1.7×10^{-4} and 0.3×10^{-4}, respectively.

The fluorescence decay and fluorescence anisotropy decays recorded for $(dT)_{20}$ by FU, which detects emission from bright excited states, did not exhibit any noticeable variation as a function of the emission wavelength. An example is shown in

dx.doi.org/10.1021/ja304069f | J. Am. Chem. Soc. 2012, 134, 14834−14845

Figure 4, where the signals obtained at 330 nm are presented together with those of TMP. Although the fluorescence decay is

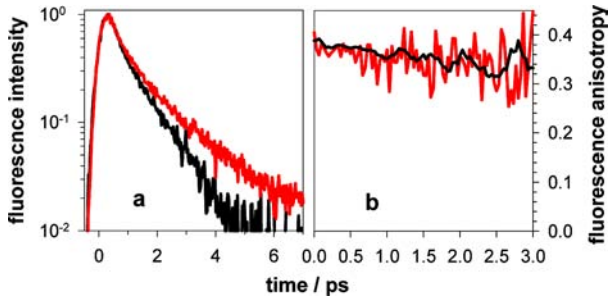

Figure 4. Fluorescence decay (a; from ref 51) and fluorescence anisotropy (b) recorded by fluorescence upconversion at 330 nm for $(dT)_{20}$ (red) and for TMP (black; from ref 4). Excitation wavelength: 267 nm.

somewhat longer than that of the nucleotide, the fluorescence anisotropy of the oligomer is practically the same as that detected for the monomer, close to 0.4. Such behavior contrasts with that of double strands, for which the ultrafast decay of fluorescence anisotropy was correlated with energy transfer involving exciton states.[4] These results show that emission correlated with delocalized Franck−Condon states is very weak.

The fluorescence decays of $(dT)_{20}$ obtained by TCSPC following excitation at 267 nm are presented in Figure 5. The

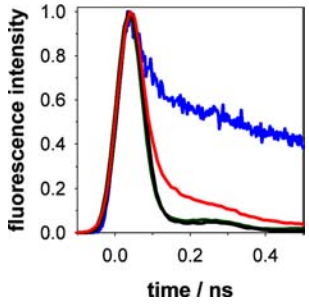

Figure 5. Fluorescence decay of $(dT)_{20}$ recorded by TCSPC at 330 (green) and 450 nm (red) following excitation at 267 nm and at 450 nm following excitation at 365 nm (blue; from ref 22). The instrumental response function is shown in black.

decay recorded at the fluorescence maximum (330 nm) is quite similar to the instrumental response function. Going to 450 nm, where contribution from the lower energy emission band (Figure 3b) is expected, the decay is still dominated by the ultrafast component detected by FU, but longer lived components appear. The contribution of long-lived components is much more important for the decay observed at the same emission wavelength when exciting at 365 nm.[22]

The quantum yield of T<>T formation, determined by combining continuous irradiation and product analysis by HPLC/MS, is shown in Figure 6. A constant $\phi_{T<>T}$ value, equal to $(5.0 \pm 0.5) \times 10^{-2}$, is found over the main absorption band. This is true for both the cis,syn and the trans,syn isomers with a ratio of 7. The same invariance of $\phi_{T<>T}$ with the irradiation wavelength was found, detecting the bleaching of the main absorption band by nanosecond flash photolysis, as described in ref 9. However, the values determined by this technique $(3.0 \pm 0.3) \times 10^{-2}$, are lower than those obtained by HPLC/MS. This discrepancy could arise from the fact that the latter method

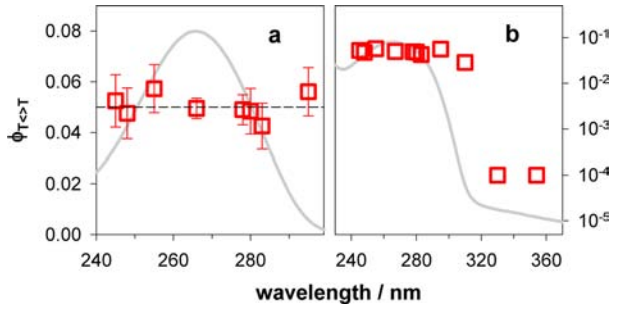

Figure 6. Wavelength dependence of the quantum yield determined for T<>T formation in $(dT)_{20}$, combining continuous irradiation and product analysis by HPLC/MS. The error bars correspond to experiments with different batches. The absorption spectrum of $(dT)_{20}$ is shown in gray.

analyzes the T<>T concentration directly whereas the former deduces it from the bleaching of the main absorption band using molar absorption coefficients of the steady-state absorption spectrum of $(dT)_{20}$. But the average ε values may not be representative of the chromophores that effectively react. Considering the $\phi_{T<>T}$ values in Figure 6 and the transient signals recorded at 280 nm, we estimate that the differential molar absorption coefficient at this wavelength is 2800 ± 1000 M^{-1} cm^{-1} whereas its average value is 5700 ± 500 M^{-1} cm^{-1}. Interestingly, heating a $(dT)_{20}$ solution from 23 °C to 92 °C increases its absorbance at 280 nm by 10%, probably because of destacking of some thymine residues. The reasons for this discrepancy are discussed in the next section. A much lower $\phi_{T<>T}$ value (7×10^{-5}) is observed upon irradiation at the weak tail of the absorption spectrum appearing in the UVA spectral domain.[22]

The quantum yield of (6-4) adducts is much lower than that of T<>Ts. Thus, to get a better picture of its variation with the irradiation wavelength, we present in Figure 7 the ratios $\phi_{6\text{-}4}/$

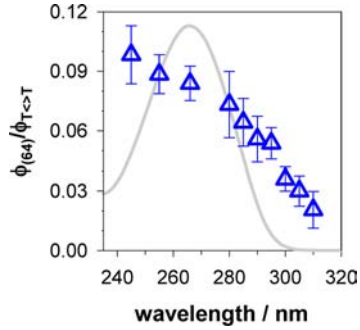

Figure 7. Ratios between the quantum yields of (6-4) adducts and T<>Ts determined following continuous irradiation of $(dT)_{20}$ at various wavelengths. The error bars correspond to experiments with different batches. The absorption spectrum of $(dT)_{20}$ is shown in gray.

$\phi_{T<>T}$. As a matter of fact, the latter are determined with experimental errors smaller than that of the absolute values. In contrast to $\phi_{T<>T}$, which is constant all over the main absorption band, $\phi_{6\text{-}4}$ continuously decreases upon increasing the irradiation wavelength, this trend being more pronounced in the red part of the spectrum. At 310 nm, $\phi_{6\text{-}4}$ is 10^{-3}. As previously reported, neither (6-4) adducts nor Dewar valence isomers could be detected following irradiation in the UVA spectral domain.[22]

dx.doi.org/10.1021/ja304069f | J. Am. Chem. Soc. 2012, 134, 14834−14845

In line with the literature, the quantum yields found for the dinucleoside monophosphate are about half of that observed for $(dT)_{20}$. Because of the lower values, the error bars associated with $\phi_{T<>T}$ and $\phi_{6\text{-}4}$ are higher for the TpT compared to that for the longer oligomer.

Neither $\phi_{T<>T}$ nor $\phi_{6\text{-}4}$ are affected by the presence of oxygen. This is valid not only for $(dT)_{20}$ but also for TpT which is more exposed to water. The absence of any oxygen effect on the photoproduct yields does not rule out the involvement of triplet states because they could react faster than the time needed for their diffusive quenching by oxygen. To further evaluate any possible involvement of the $^3\pi\pi^*$ state in T<>T formation, we also examined the dependence of the intersystem crossing quantum yield ϕ_{ISC} on the excitation wavelength. This was done by nanosecond flash photolysis for TMP because no triplet absorption is detected by this technique for $(dT)_{20}$.[9] As a matter of fact, transient absorption experiments with femtosecond resolution using 267 nm excitation showed that the lifetime of the $^3\pi\pi^*$ state in $(dT)_{20}$ is 140 ps.[11] At this excitation wavelength, both the triplet absorption spectrum and the intersystem crossing quantum yields ϕ_{ISC} found for the monomer and the oligomer are similar.[11] Thus, we can reasonably estimate the excitation wavelength dependence of ϕ_{ISC} for $(dT)_{20}$ by studying that of TMP.

We recorded the decays of the TMP triplet absorption at 360 nm, corresponding to the maximum of its spectrum,[52,53] at various excitation wavelengths between 248 and 283 nm (Figure 8b); ϕ_{ISC} was determined from the zero-time

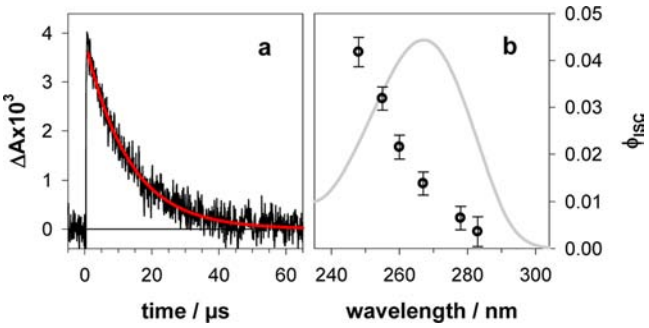

Figure 8. Properties of the $^3\pi\pi^*$ state determined for TMP in water by nanosecond flash photolysis: (a) decay at 360 nm following excitation at 248 nm, fitted by a monoexponential function (τ = 13 μs); (b) quantum yield of intersystem crossing as a function of the excitation wavelength. The absorption spectrum of TMP is shown in gray.

differential absorbance[9] using a molar absorption coefficient of 2300 M^{-1} cm^{-1}.[53] We found that ϕ_{ISC} decreases considerably with increasing excitation wavelength: for the examined excitation range, ϕ_{ISC} values span 1 order of magnitude, decreasing to 4×10^{-3} at the red part of the spectrum (Figure 8b). From the concentration dependence of the TMP triplet decays, we found a self-quenching constant of $(4 \pm 1) \times 10^7$ M^{-1} s^{-1}), which is in fairly good agreement with that obtained via triplet photosensitization.[53]

COMPUTATIONAL RESULTS

In this section, we first present the results obtained for the dimerization of two stacked thymines in the gas phase, checking the reliability of our approach in comparison with higher level calculations. Then, we examine the TpT in water. A thorough analysis of the absorption spectra and the main nonradiative decay pathways found for several conformers of TpT will be reported in a forthcoming study.[24] Here, we present the main features of the Franck−Condon states and focus on the paths leading to T<>T or oxetane formation.

Photodimerization of Two Stacked Thymines in the Gas Phase. To verify if TD-M052X calculations can provide a qualitatively correct description of the dimerization process and to better appreciate the effect of the backbone and the solvent on the photoinduced processes, we performed several test calculations on two stacked thymines in the gas phase, for which a comparison with MCSCF ab initio calculations is possible. As a first step, we performed single point TD-M052X/6-31G(d) calculations on the MECI leading to the T<>T dimer, optimized by Blancafort and Migani at the CASSCF(12/12)/6-31G(d) level,[12] obtaining a very small S_0-S_1 energy gap, only ca. 0.55 eV. Analogously, the S_0-S_1 energy gap in the MECI[54] leading to the oxetane predicted by TD-M052X level is only 0.8 eV. These energy gaps are also similar to those obtained by Blancafort and Migani[12] when refining, at the CASPT2 level, the energy of the CI located at the CASSCF level.

The above comparison clearly indicates that the location of the crossing region leading to the T<>T and to the oxetane intermediate is predicted correctly by TD-M052X. The reliability of the latter method was further investigated by optimizing the energy of the lowest energy singlet excited state of a symmetric face-to-face thymine pair, which, according to Serrano-Perez et al.[55] should be the ideal one for the formation of stable excited dimers. The starting point was an intermonomer distance of 3.6 Å, i.e., similar to that of two neighboring thymines located on the same DNA strand. TD-M052X/6-31+G(d,p) geometry optimizations of the lowest energy singlet excited-state predict that a barrierless path leads to a region exhibiting a relatively low energy gradient (ca. 0.0025 au), characterized by small stacking distances (Figure 9)

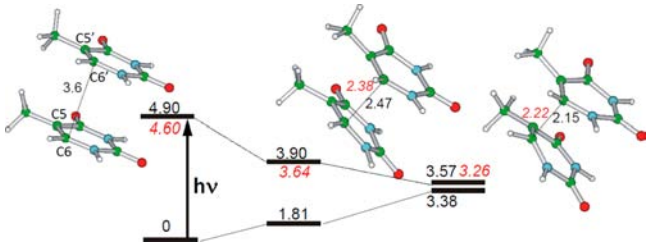

Figure 9. Schematic description of the most relevant points of the path leading to the T<>T formation after UV excitation of a pair of stacked thymines in the gas phase, as computed at the TD/M052X/6-31G(d) level. In red are reported the values obtained at the CASPT2(12/12)/ANO level.[55].

and an initial pyramidalization at C5 and C6 atoms. Excited-state geometry optimizations then lead to a region of the PES where S_1 and S_0 are close to degeneracy, providing very short C6−C6′ and C5−C5′ bond distances. The lowest energy point found in this region is shown in Figure 9 together with the corresponding bond distance of the CI for the T<>T formation located at the CASSCF/(12/12)/ANO level by Serrano-Perez et al.[55]

From the energetic point of view, the picture provided by TD-M052X is very similar to that of CASPT2(12/12)/ANO calculations. Indeed, although the absorption energy ν_A is ca.

dx.doi.org/10.1021/ja304069f | J. Am. Chem. Soc. 2012, 134, 14834−14845

0.3 eV higher at the TD/M052X/6-31+G(d,p) level, the S_1 PES is almost parallel to the CASPT2 one. The excited dimer minimum is ca. 1 eV more stable than the FC point, and the CI is ca. 0.35 eV more stable than the excited dimer minimum. The structural features of the CI located at the CASSCF/(12/12)/ANO level are also similar to that of the S_1/S_0 crossing region located at the TD/M052X level. Briefly, our analysis indicates that the picture of the photodimerization process provided by TD-M052X on two stacked thymines in the gas phase is very similar to that obtained at the CASPT2 level for what concerns the formation of both T<>T and oxetane intermediate.

Absorption Spectrum of TpT in Water. The main features of TpT absorption spectrum in water, predicted by TD-M052X/6-31G(d) calculations, do not depend on the backbone conformation. As an example, we present in Figure 10 the spectrum computed for the C2endo−C2endo conformer.

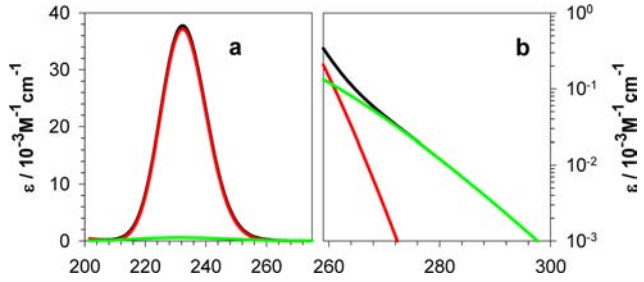

Figure 10. (a) Absorption spectra computed in water for the c2endo−c2endo TpT conformer (black) by convoluting each transition by a Gaussian function with a width (fwhm) of 0.2 eV for "neutral" transitions (red) and 0.4 eV for CT transitions (green). (For further details, see Supporting Information). (b) A close-up of the red wing.

Because of the dipolar coupling, the two bright $^1\pi\pi^*$ transitions are no longer degenerate and exhibit different intensities, that located at higher energy having the strongest oscillator strength. The exciton splitting ranges from 0.1 to 0.25 eV, the largest value corresponding to the C3endo−C3endo conformer.[24]

The computed vertical excitation energies are noticeably blue-shifted with respect to the experimental absorption maxima. However, previous studies indicate that using a more extended basis set,[56,57] including explicit solute−solvent interactions[56,57] and considering vibrational effects on the absorption spectrum[58] would cause a significant red-shift of the computed band, improving the agreement with experimental results. On the other hand, for the purposes of the present study, it is more important that our calculations are able to correctly reproduce the effect of the stacking on the excited states than being in absolute agreement with the experimental spectra. In this respect, comparison with experiments and with CASPT2 calculations indicate that our simpler approach, based on PCM/M052X/6-31G(d) calculations and allowing a more extensive exploration of the relevant PES, is fully adequate.

Two $^1n\pi^*$ transitions, localized on the two thymine moieties, have a transition energy very close to that of their counterpart in noninteracting mononucleotides and fall very close to the lower exciton state. However, previous studies on thymine indicate that extension of the basis set size and inclusion of solute−solvent hydrogen bonding interactions decrease its relative stability with respect to $^1\pi\pi^*$ transitions.[56] Indeed, when using the 6-311+G(2d,2p) basis set on a computational model including four water molecules of the cybotactic region, the $^1n\pi^*$ transition is destabilized by 0.4 eV with respect to the $^1\pi\pi^*$ bright state.[56] These indications are confirmed by test calculations on a model system including TpT and eight water molecules.[24] Therefore, we evaluate that the energy of the $^1n\pi^*$ transitions is significantly higher by 0.4−0.5 eV than that corresponding to the lower energy $^1\pi\pi^*$ excitons; they fall 0.3 eV on the blue with respect to the maximum of the absorption band, and they should not be significantly populated following UV absorption.

At the SS-PCM/TD-M052X level, thymine→thymine CT transitions are blue-shifted by 0.2−0.3 eV with respect to the maximum of the absorption band. The calculation of the inhomogeneous broadening according to the procedure described in Computational Details shows that CT transitions are characterized by large inhomogeneous broadening and their relative contribution to the red wing of the absorption spectrum is concomitantly large (Figure 10). Solvent effects for an oligonucleotide, which is a strongly charged system, are not easily modeled. This is especially true for CT transitions, whose energy could be very sensitive to metal ion or backbone fluctuations, further increasing their spectral broadening. Consequently, our estimate provides a lower limit to the effective broadening experienced by a CT transition which does not affect our qualitative conclusion. Finally, the spectral width of CT transitions in stacked dinucleotides obtained by QM/MM approaches, explicitly including solvent molecules, is similar to our estimate.[7] The above picture is still valid when the Na^+ counterion is explicitly included in the calculations.

Photodimerization of TpT in Water. *T<>T Formation.* PCM/TD-M052X/6-31G(d) calculations indicate that, for several TpT conformers, barrierless paths do exist, leading from the Franck−Condon region of the exciton states to a crossing region with S_0 or to a relaxed $^1\pi\pi^*$ exciton minimum, characterized by very short intermonomer distances.

In the former case, we found a strong decrease in the C5C6/C5′C6′ bonds: the C6−C6′ distance diminishes until a CI region is found, as indicated by the very low S_1/S_0 energy gap (<0.7 eV) and by the severe convergence problems of the LR-PCM/TD-M052X/6-31G(d) geometry optimization. Figure 11 shows a representative of the dinucleotide structure at the conical intersection region (T<>T-CI*). It is very similar to that found for isolated stacked thymines in the path leading to

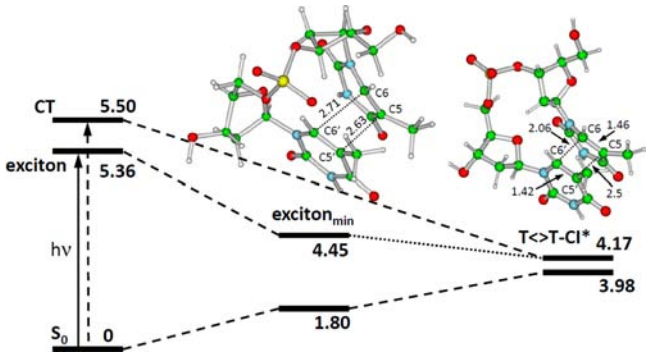

Figure 11. T<>T reaction path. Structures and relative energies of some representative points in the path leading to the formation of T<>T for TpT as predicted by PCM/TD-M052X/6-31G(d) calculations: relaxed exciton minimum ($exciton_{min}$), representative structure of the S_0/S_1 crossing region (T<>T-CI*).

dx.doi.org/10.1021/ja304069f | J. Am. Chem. Soc. 2012, 134, 14834−14845

T<>T: the C5−C5′ and, especially, the C6−C6′ distances are very short, e.g., 2.5 Å and 2.06 Å, respectively. Moreover, the C5−C6 distance (1.46 Å) is quite close to that of a single CC bond, indicating the incipient T<>T formation. Starting from T<>T-CI*, we performed a PCM/M052X/6-31G(d) ground-state geometry optimization, which converges to the T<>T minimum. This result confirms that the region around T<>T-CI* belongs to the T<>T reactive path. Note that excited-state geometry optimization including the Na^+ ion provides a picture similar to that just described, predicting a barrierless decay to the CI in the path leading to T<>T formation. A representative structure in this path, where the S_0/S_1 energy gap is only 0.19 eV, is shown in Figure 11.

For the conformers where at least one of the rings adopts the C3-endo conformation, bright excitons are predicted to decay to a minimum ($exciton_{min}$) characterized by very short intermonomer distances and long C5−C6 bond distances (Figure 11) and low emission energies (ca. 2.7 eV). However, an extensive exploration of the PES[24] indicates that these minima are separated by a very small energy barrier from the crossing region with S_0. We note that thermal fluctuations of the backbone would reinforce decay toward the conical intersection. Actually, the $exciton_{min}$ is less stable than the T<>T-CI*, indicating that the $exciton_{min}$→T<>T-CI* transition is exergonic.

Formation of the Oxetane Intermediate. Optimization of the thymine → thymine CT state at the LR-PCM/TD-M052X/6-31G(d) level leads to sudden decay to bright excitons.[24] This result is not surprising, because the stability of the CT states is known to be underestimated by LR-PCM/TD-M052X calculations.[6,32,33] Unfortunately, excited geometry optimizations at the SS-PCM level are not feasible. As a consequence, to get an estimate of the structural features of CT-state minima, we performed LR-PCM/PBE0 geometry optimizations, exploiting the fact that the overestimation of the CT stability by PBE0 makes geometry optimizations less cumbersome. PBE0 geometry optimizations predict that the most significant geometrical changes involve intramonomer degrees of freedom, one of the thymines adopting the geometry of a cation and the other of an anion. Our calculations predict that the final outcome of the geometry optimization will depend on the backbone conformation and on the CT directionality (i.e., if it is in the direction $5'^{+}$→$3'^{-}$ or $3'^{-}$→$5'^{+}$). When both sugar rings adopt the C2 endo puckering and for the $5'^{+}$→$3'^{-}$ CT state, LR-PCM/TD-PBE0/6-31G(d) calculations predict that the O8′ atom approaches the C5 atom, as in a nucleophilic attack of the negative moiety toward the positive one, reaching a pseudominimum[24] denoted by CT_{min}*, in Figure 12. The latter is characterized by significant changes in the backbone dihedral angles. Subsequent LR-PCM/TD-M052X geometry optimization leads to another crossing region with S_0. This structure lies in the path leading to the formation of the oxetane intermediate (OXET-CI* in Figure 12), which was also found for stacked thymines in the gas phase. In the OXET-CI* region, O8′ is very close to C5 (1.65 Å) and C4′ is approaching C6 (2.46). Moreover, C5−C6 and C4′−O8′ distances, 1.45 Å and 1.34 Å, respectively, approach typical values of standard CC and CO single bonds. Not surprisingly, it is sufficient to decrease the O8′−C5 distance by 0.1 Å only to allow ground-state M052X/6-31G(d) geometry optimizations starting from OXET-CI* to converge to a stable oxetane minimum.

Oxetane formation leads to a decrease of the dipole moment, which is particularly strong for the CT_{min}* (18.3 D). As

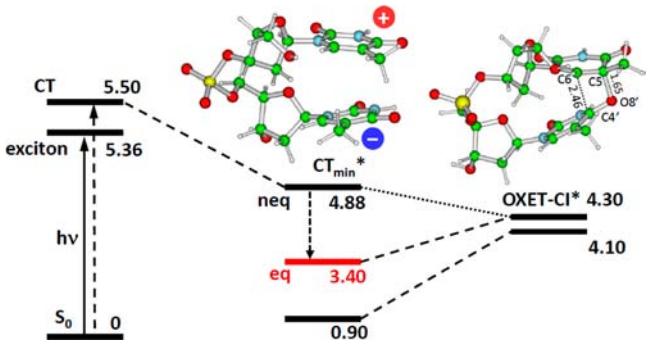

Figure 12. Oxetane reaction path. Structures and relative energies of some representative points in the path leading to oxetane in TpT, as predicted by PCM/TD-M052X/6-31G(d) calculations: minimum of the 5′→3′ CT state (CT_{min}*, TD-PBE0 calculations), representative structure of the S_0/S_1 crossing region (OXET-CI*).

confirmed by a very recent paper on excited-state proton transfer in the guanine-cytosine base pair,[59] LR-PCM/TD-DFT calculations are not suitable for describing processes involving large electronic density shifts and requiring an accurate treatment of the dynamical solvation effects (for example, the solvent reorganization energy). Therefore, we refined the energy of CT_{min}* and OXET-CI* at the SS-PCM level. OXET-CI* is so close to S_0 that the iterative procedure of SS-PCM/TD-DFT calculations cannot converge; the system oscillates between two different excited states. As a consequence, we made SS-PCM/TD-M052X computations for a structure in the path leading to OXET-CI* (S_1/S_0 energy gap ca. 1 eV) and corrected the final results for the energy difference between this structure and OXET-CI*. At the LR-PCM/TD-M052X level, OXET-CI* is more stable than CT_{min}* by ca. 1 eV. This value decreases to ca. 0.45 eV, by performing SS-PCM/TD-M052X/6-31G(d) at the solvent "neq" level. Finally, when solvent degrees of freedom are fully equilibrated with the excited electron density, the CT_{min}* → OXET-CI* transition is predicted to be significantly endergonic (by ca. 0.75−1 eV).

Because the CT_{min}* has not been optimized by M052X functionals, these values provide only a lower limit. Furthermore, the relaxed CT state found for TpT in water may be less stable than that in $(dT)_{20}$, in which thymine residues are less exposed to water molecules. To estimate this effect, we performed calculations using smaller dielectric constants, 4 and 8. In both cases, CT_{min}* is more stable than OXET-CI* by 0.12 and 0.45 eV, respectively. Although only a fully quantum dynamical study, rigorously including the coupling between solute and solvent degrees of freedom also in the proximity of the CI,[40] can provide an accurate picture of the oxetane formation starting from the CT state and although reaction dynamics is expected to be modulated also by explicit solute−solvent interactions and the fluctuations of the charged moieties of the oligonucleotide backbone, our calculations strongly suggest that a non-negligible energy barrier is associated with the path leading to the oxetane formation. Because CT excited states are formed on a subpicosecond time scale, faster than vibrational cooling,[60] their reactivity could be sensitive to the excess energy deposited on the molecule, in line with the observed dependence of $\phi_{6\text{-}4}$ on the excitation wavelength. Also in this case, we have verified that the inclusion of the Na^+ counterion does not significantly affect the path leading to oxetane formation.

dx.doi.org/10.1021/ja304069f | J. Am. Chem. Soc. 2012, 134, 14834−14845

DISCUSSION

In this section we first discuss the spectral properties of $(dT)_{20}$ in light of our quantum chemical calculations. Then, we focus on cycloadditions leading to cyclobutane dimers and (6-4) adducts. Finally we comment on the role played by triplet states.

Spectral Properties. Our calculations were performed for the dinucleotide monophosphate TpT in which thymines are stacked, close to what is expected for double-stranded DNA. Such geometrical arrangement favors cooperative effects arising from the electronic coupling, dipolar and due to orbital overlap. Experimentally, these effects are very difficult to study for TpT. Although not large, they are detectable in the absorption and fluorescence properties of $(dT)_{20}$. But even long thymine strands are known to exhibit important structural disorder.[61] Consequently, the electronic coupling is expected to concern only a small part of bases in $(dT)_{20}$. This is reflected in the fluorescence anisotropy measured on the femtosecond time scale, which is as high as that of the mononucleotide (Figure 4b), even after 1 ps, when the oligomer decay deviates from that of the monomer. Therefore, we conclude that, for the major part of the bases, photon emission is not preceded by energy transfer. Such behavior contrasts with that of DNA duplexes for which ultrafast excitation energy transfer, possibly via population of delocalized Franck−Condon states, is observed.[4,23] Evidently, photon emission is quenched by the dimerization reactions, affecting in total about 11% of the chromophores, when excited near to the absorption maximum (Figures 6 and 7); this percentage is deduced from the sum of $\phi_{T<>T}$ (0.05) and $\phi_{6\text{-}4}$ (0.005) multiplied by two, because the formation of each dimeric photoproduct leads to the disappearance of two thymine residues. Consequently, the weak spectral shift observed between the absorption of TMP and $(dT)_{20}$, in connection with practically identical properties for their $^1\pi\pi^*$ fluorescence, peaking at 330 nm (Figures 3 and 4), suggest that coupled chromophores do not significantly contribute to this emission band.

The fingerprint of the electronic coupling is found in the low energy emission band, which is absent from the spectrum of TMP. The photophysical properties associated with UVA absorption have been the subject of a previous experimental study which compared the behavior of the duplex $(dA)_{20}\cdot(dT)_{20}$ with that of the parent single strands $(dA)_{20}$ and $(dT)_{20}$.[22] It was shown that base-pairing leads to an increase in the intensity of the UVA absorption, the fluorescence quantum yield, and the fluorescence lifetime which decays on the nanosecond time scale. The radiative lifetimes suggest emission from weakly allowed transition, which had been associated with charge transfer transitions. Indeed, it is unlikely that $\pi\pi^*$ excitons are encountered at such low energies because the electronic coupling between dipolar $\pi\pi^*$ transitions for stacked or paired bases does not exceed a few hundreds of wavenumbers.[8,62] Furthermore, $n\pi^*$ states, which have the lowest energy for DNA bases in the gas phase, are expected to be strongly destabilized in the presence of water molecules,[63] but UVA absorption and related emission also concern dinucleotides which are exposed to water.[64] Finally, a recent study on hairpins has shown that the UVA absorption depends on the redox potential of the bases, corroborating the attribution to CT transitions.[65]

The resemblance of the low energy emission band, observed for $(dT)_{20}$ upon UVC excitation, to that obtained upon UVA excitation[22] suggests emission from the same type of excited states. Population of the CT states associated with different Franck−Condon conformations may lead to the same fluorescence band if this stems from the minimum of the potential energy surface.

Cyclobutane Dimer Formation. Our theoretical study has shown that T<>T formation takes place from the $^1\pi\pi^*$ excitons (Figure 11), whose fingerprint is detected in the absorption spectrum. We demonstrate that neither steric hindrance, caused by the presence of the backbone, nor the existence of the counterion perturbs the reaction path. Moreover, the absorption associated with the excitons strongly overlaps that of the localized $^1\pi\pi^*$ transitions. Finally, there is no hint of any energy barrier along the [2 + 2] dimerization path. These computational results are in line with the experimental observation that the T<>T quantum yield remains constant for irradiation across the main absorption band of both TpT and $(dT)_{20}$, the latter being about twice as high as the former.

Another experimental indication corroborating T<>T formation from exciton states is provided by the molar extinction coefficient of that thymines that effectively react. These values (e.g., 2800 ± 1000 M^{-1} cm^{-1} at 280 nm), deduced from flash photolysis experiments and determined by HPLC/MS, are much lower compared to the average values corresponding to the steady-state absorption spectrum (5700 ± 500 M^{-1} cm^{-1} at 280 nm). Our calculations indeed show that the spectrum of coupled thymines is characterized by a hypochromism compared to that of uncoupled chromophores, as happens in double-stranded structures.

Our results concerning T<>T formation upon irradiation of $^1\pi\pi^*$ states are in agreement with the model developed by Schatz and Lewis, according to which only pairs of thymines characterized by an appropriate distance between the reactive bonds in their ground-state conformation react.[14] For such close-lying chromophores, the dipolar coupling is sufficiently strong as to give rise to delocalized excited states. Moreover, our results strongly corroborate the conclusions drawn from ultrafast spectroscopy with infrared detection, according to which T<>T formation in thymine strands is an ultrafast process.[10]

T<>T formation is also induced following UVA irradiation (Figure 6b).[22] The abrupt decrease observed in $\phi_{T<>T}$ when going from the main absorption band to the red tail shows that different types of excited states are involved in [2 + 2] dimerization. Following the reasoning developed previously (see Spectral Properties), the weak red tail appearing in the absorption spectrum of stacked thymines is attributed to CT transitions (Figure 10). Interconversion between CT and $^1\pi\pi^*$ states is possible through vibronic coupling, as shown to occur in the case of stacked adenines,[33,66] and stacked cytosines, according to a recent dynamical study of T<>T formation.[67] The possibility of an interconversion between $^1\pi\pi^*$ and CT transitions is corroborated by the overlap of their fluorescence bands. However, the probability that $^1\pi\pi^*$ states are thus repopulated is not high. Taking into account the additional requirement of appropriate geometry for the thymine pair to react, the very low $\phi_{T<>T}$ values observed following UVA irradiation are understandable.

Focusing on the $^3\pi\pi^*$, we assume that ϕ_{ISC} found for TMP (Figure 8b) is representative for the intersystem crossing in $(dT)_{20}$, because the major part of its thymines behave as monomeric chromophores. The strong wavelength dependence of ϕ_{ISC} (Figure 8b) clearly contrasts with the invariability of

$\phi_{T<>T}$ (Figure 6a). Taking into account the experimental errors, we conclude that the contribution of $^3\pi\pi^*$ states to T<>T formation should be lower than 10%. Consequently, thymine dimerization is not responsible for the rapid decay of $^3\pi\pi^*$ in $(dT)_{20}$, which is probably due to self-quenching. The latter issue was discarded[11] on the basis of the self-quenching constants determined for the TMP $^3\pi\pi^*$.[52,53] The equation used for this purpose is valid only for chromophores undergoing three-dimensional isotropic diffusion. Therefore, its application to multichromophoric systems is irrelevant.

Formation of (6-4) Adducts. The dependence of $\phi_{6\text{-}4}$ on the irradiation wavelength (Figure 7) could be due to the involvement of an excited state whose population depends on the excitation energy or/and because the reaction must overcome an energy barrier. One possibility, discussed in the past, is oxetane formation via $n\pi^*$ states.[20] Transient absorption experiments revealed that $n\pi^*$ is formed with a quantum yield of 10% upon excitation of TMP at 267 nm and decay with a time constant of 127 ps.[68] Furthermore, experiments revealed a much higher quantum yield for uracil monophosphate (UMP; 42%) than for TMP.[68] Despite this fact, the quantum yield of (6-4) adducts in the uracil dinucleotide is lower by 1 order of magnitude compared to that found for the corresponding thymine dinucleotide.[69] Consequently, the involvement of the $n\pi^*$ state in the (6-4) dimerization is unlikely. Moreover, according to our calculations, $n\pi^*$ states decay to the ground state without any hint for oxetane formation. Finally, neither was a reaction path toward the oxetane intermediate found in the $^1\pi\pi^*$ states.

In contrast, our calculations provide strong indications that oxetane is formed via excited charge transfer states involving two thymines. Due to the presence of the backbone and the solvent, the CT states move to lower energies compared to that for the gas phase.[12] An energy barrier, arising mainly from dynamical solvent effects, is predicted, as dependence of $\phi_{6\text{-}4}$ induction on excitation wavelength (Figure 7). The existence of such a barrier supports the fact that, although CT states could be directly populated in the UVA spectral domain, no (6-4) adducts are detected for these irradiation wavelengths, not only in $(dT)_{20}$ but also in $(dA)_{20}\cdot(dT)_{20}$ and natural DNA.

Note that the agreement between the experimental values and the quantum yields calculated according to the Lewis and Schatz model is not as good for (6-4) adducts as compared to that for T<>Ts.[14] The assumption used in this model is that (6-4) dimerization is governed by the ground-state geometry which contrasts with both the wavelength dependence of $\phi_{6\text{-}4}$ found here (Figure 7) and the existence of an energy barrier for this reaction determined from our quantum chemical calculations.

CONCLUSION

In this paper we report a joint experimental and computational study of dimer formation in thymine single strands. The described steady-state and time-resolved optical properties of $(dT)_{20}$ and PCM/TD-M052X calculations on TpT provide complementary information about the main UV-induced dimerization paths, leading to cyclobutane dimers and (6-4) adducts, and offer novel insights regarding the excited states thereby involved.

The dependence of the quantum yield on the irradiation wavelength, determined experimentally for the formation of cyclobutane dimers and (6-4) adducts, implies that each reaction involves completely different excited states or different paths to the same excited state, one barrierless and the other with an energy barrier. Both possibilities are new with respect to recent interpretative models, which so far have focused mainly only the role of the ground-state conformation.[14] Moreover, our experimental results clearly demonstrate that the contribution of the $^3\pi\pi^*$ state to the [2 + 2] cycloaddition, largely discussed in the past and brought recently to the forefront,[11] is less than 10%.

Our quantum mechanical calculations, which are the first to consider explicitly the influence of the backbone and the solvent, show that (6-4) adducts and cyclobutane dimers originate from two different excited states. The [2 + 2] dimerization takes place via $^1\pi\pi^*$ excitons and proceeds along a barrierless path. The formation of oxetane, i.e., the putative reaction intermediate leading to (6-4) adducts, occurs via charge transfer excited states involving the two thymines and must overcome an energy barrier.

According to the theoretical results, both reactions involve strongly coupled thymines. The fingerprint of electronic coupling is indeed detected in the experimental steady-state absorption and fluorescence spectra of $(dT)_{20}$. The latter show that charge transfer states can be populated following excitation near the absorption maximum. Furthermore, the determined molar absorption coefficients combined with steady-state measurements and flash photolysis experiments reveal an important hypochromism of the reacting thymines, typical of stacked bases in double-stranded DNA.

Although experiments and calculations provide a consistent and convergent picture, it is not yet possible to make a quantitative comparison between them. We are indeed aware that the simple existence of barrierless excited-state paths does not automatically imply ultrafast and effective photoreactive paths, and vice versa. In this respect, our calculations suggest that the vibronic coupling between $^1\pi\pi^*$ excitons and charge transfer states plays an important role in modulating the excited-state reactivity, confirming the importance of non-adiabatic couplings in the outcome of photoactivated processes. Only a fully quantum dynamical study, at the moment out of reach for a system as complex as an oligonucleotide in solution, could provide results to directly compare with the experimental results.[66,70] Furthermore, calculations concern the dinucleoside monophosphate whereas experiments are mainly carried out for the eicosamer $(dT)_{20}$. However, the similarity (within a factor two) of $\phi_{T<>T}$ and $\phi_{6\text{-}4}$ in $(dT)_{20}$ and TpT suggests that the analysis carried out for the dinucleotide describes the processes occurring in larger systems reasonably well.

In the present work we discussed the electronic excited states responsible for direct UV-induced damage to DNA. We found that, in this type of damage, reactions proceeding via triplet states do not play a key role. The picture is different for indirect damage; T<>T formation via triplet sensitization is well established,[1,2] but even in this case, collective effects are expected to be quite important. As a matter of fact, the energy of the "thymine triplet" within DNA is much lower than that of TMP.[2] It would not be surprising if such a triplet state corresponds in fact to charge transfer excited states lying much below the $\pi\pi^*$ states.

ASSOCIATED CONTENT

Supporting Information

Further information on quantum mechanical calculations. Complete Gaussian reference (ref 44 in the manuscript).

This material is available free of charge via the Internet at http://pubs.acs.org.

AUTHOR INFORMATION

Corresponding Author

robimp@unina.it; dimitra.markovitsi@cea.fr

Present Address

[⊥]Laboratoire de Chimie Physique, CNRS UMR 8000, Université Paris-Sud, F-91405 Orsay, France.

Notes

The authors declare no competing financial interest.

ACKNOWLEDGMENTS

The French Agency for Research (ANR-10-BLAN-0809-01) and the Conselleria de Educacion-Generalitat Valenciana (VALi +D program to I.V., no. 2010033). R.I. thanks MIUR (PRIN 2008 and FIRB Futuro in Ricerca 2008) for financial support.

REFERENCES

(1) Ravanat, J. L.; Douki, T.; Cadet, J. *J. Photochem. Photobiol., B* **2001**, *63*, 88−102.

(2) Bosca, F.; Lhiaubet-Vallet, V.; Cuquerella, M. C.; Castell, J. V.; Miranda, M. A. *J. Am. Chem. Soc.* **2006**, *128*, 6318−6319.

(3) Bouvier, B.; Gustavsson, T.; Markovitsi, D.; Millié, P. *Chem. Phys.* **2002**, *275*, 75−92. Buchvarov, I.; Wang, Q.; Raytchev, M.; Trifonov, A.; Fiebig, T. *Proc. Natl. Acad. Sci. U.S.A.* **2007**, *104*, 4794−4797. Bittner, E. R. *J. Photochem. Photobiol., A* **2007**, *190*, 328−334. Burin, A. L.; Dickman, J. A.; Uskov, D. B.; Hebbard, C. F. F.; Schatz, G. C. *J. Chem. Phys.* **2008**, *129*, 091102. Starikov, E. B.; Cuniberti, G.; Tanaka, S. *J. Phys. Chem. B* **2009**, *113*, 10428−10435. Burin, A. L.; Armbruster, M. E.; Hariharan, M.; Lewis, F. D. *Proc. Natl. Acad. Sci. U.S.A.* **2009**, *106*, 989−994.

(4) Markovitsi, D.; Onidas, D.; Gustavsson, T.; Talbot, F.; Lazzarotto, E. *J. Am. Chem. Soc.* **2005**, *127*, 17130−17131.

(5) Crespo-Hernández, C. E.; Cohen, B.; Kohler, B. *Nature* **2005**, *436*, 1141−1144. Markovitsi, D.; Talbot, F.; Gustavsson, T.; Onidas, D.; Lazzarotto, E.; Marguet, S. *Nature* **2006**, *441*, E7.

(6) Santoro, F.; Barone, V.; Improta, R. *J. Am. Chem. Soc.* **2009**, *131*, 15232−15245.

(7) Lange, A. W.; Herbert, J. M. *J. Am. Chem. Soc.* **2009**, *131*, 3913−3922.

(8) Kozak, C. R.; Kistler, K. A.; Lu, Z.; Matsika, S. *J. Phys. Chem. B* **2010**, *114*, 1674−1683.

(9) Marguet, S.; Markovitsi, D. *J. Am. Chem. Soc.* **2005**, *127*, 5780−5781.

(10) Schreier, W. J.; Schrader, T. B.; Koller, F. O.; Gilch, P.; Crespo-Hernàdes, C.; Swaminathan, V. N.; Carell, T.; Zinth, W.; Kohler, B. *Science* **2007**, *315*, 625−629. Schreier, W. J.; Kubon, J.; Regner, N.; Haiser, K.; Schrader, T. E.; Zinth, W.; Clivio, P.; Gilch, P. *J. Am. Chem. Soc.* **2009**, *131*, 5038−5039.

(11) Kwok, W. M.; Ma, C.; Phillips, D. L. *J. Am. Chem. Soc.* **2008**, *130*, 5131−5139.

(12) Blancafort, L.; Migani, A. *J. Am. Chem. Soc.* **2007**, *129*, 14540−14541.

(13) Law, Y. K.; Azadi, J.; Crespo-Hernandez, C. E.; Olmon, E.; Kohler, B. *Biophys. J.* **2008**, *94*, 3590−3600.

(14) McCullagh, M.; Lewis, F.; Markovitsi, D.; Douki, T.; Schatz, G. C. *J. Phys. Chem. B* **2010**, *114*, 5215−5221.

(15) Zhang, R. B.; Eriksson, L. A. *J. Phys. Chem. B* **2006**, 7556−7562. Climent, T.; Gonzalez-Ramirez, I.; Gonzalez-Luque, R.; Merchan, M.; Serrano-Andres, L. *J. Phys. Chem. Lett.* **2010**, *1*, 2072−2076.

(16) Varghese, A. J.; Wang, S. Y. *Science* **1967**, *156*, 955.

(17) Clivio, P.; Fourrey, J.-L.; Gasche, J. *J. Am. Chem. Soc.* **1991**, *113*, 5481−5483.

(18) Deering, R. A.; Setlow, R. B. *Biochem. Biophys. Acta* **1963**, *68*, 526−534.

(19) Johns, H. E.; Pearson, M. L.; LeBlanc, J. C.; Helleiner, C. W. *J. Mol. Biol.* **1964**, *9*, 503−524. Garcés, F.; Dávila, C. A. *Photochem. Photobiol.* **1982**, *35*, 9−16.

(20) Lemaire, D.; Ruzsicska, B., P. *Photochem. Photobiol.* **1993**, *57*, 755−769.

(21) Yang, Z. B.; Zhang, R. B.; Eriksson, L. A. *Phys. Chem. Chem. Phys.* **2011**, *13*, 8961−8966.

(22) Banyasz, A.; Vayá, I.; Changenet-Barret, P.; Gustavsson, T.; Douki, T.; Markovitsi, D. *J. Am. Chem. Soc.* **2011**, *133*, 5163−5165.

(23) Markovitsi, D.; Gustavsson, T.; Banyasz, A. *Mutat. Res., Rev. Mutat. Res.* **2010**, *704*, 21−28.

(24) Improta, R. To be submitted.

(25) Velapoldi, R. A.; Mielenz, K. D. *A fluorescence standard reference material: quinine sulfate dihydrate*; U.S. Government Printing Office: Washington, D.C., 1980.

(26) Onidas, D.; Markovitsi, D.; Marguet, S.; Sharonov, A.; Gustavsson, T. *J. Phys. Chem. B* **2002**, *106*, 11367−11374.

(27) Rahn, R. O.; Sellin, H. G. *Photochem. Photobiol.* **1979**, *30*, 317−318.

(28) Gustavsson, T.; Sharonov, A.; Onidas, D.; Markovitsi, D. *Chem. Phys. Lett.* **2002**, *356*, 49−54.

(29) Douki, T.; Cadet, J. *Biochemistry* **2001**, *40*, 2495−2501.

(30) Zhao, Y.; Schultz, N. E.; Truhlar, D. G. *J. Chem. Theory Comput.* **2006**, *2*, 364−382.

(31) Zhao, Y.; Truhlar, D. G. *Acc. Chem. Res.* **2008**, *41*, 157−167.

(32) Improta, R. *Phys. Chem. Chem. Phys.* **2008**, *10*, 2656−2664.

(33) Improta, R.; Barone, V. *Angew. Chem., Int. Ed.* **2012**, 12016−12019.

(34) Adamo, C.; Scuseria, G. E.; Barone, V. *J. Chem. Phys.* **1999**, *111*, 2889−2899.

(35) Tomasi, J.; Mennucci, B.; Cammi, R. *Chem. Rev.* **2005**, *105*, 2999−3093.

(36) Cossi, M.; Barone, V. *J. Chem. Phys.* **2001**, *115*, 4708−4717.

(37) Scalmani, G.; Frisch, M. J.; Mennucci, B.; Tomasi, J.; Cammi, R.; Barone, V. *J. Chem. Phys.* **2006**, *124*, 094107.

(38) Improta, R.; Barone, V.; Scalmani, G.; Frisch, M. J. *J. Chem. Phys.* **2006**, *125*, 051103.

(39) Improta, R.; Scalmani, G.; Frisch, M. J.; Barone, V. *J. Chem. Phys.* **2007**, *127*, 074504.

(40) Burghardt, I.; Hynes, J. T. *J. Phys. Chem. A* **2006**, *110*, 11411−11423. Laage, D. B., I.; Hynes, T. J. In *Continuum Solvation Models in Chemical Physics: Theory and Application*; Cammi, R., Mennucci, B., Eds.; Wiley-VCH: Weinheim, 2007; p 429. Toniolo, A.; Olsen, S.; Manohar, L.; Martınez, T. J. *Faraday Discuss.* **2004**, *127*, 149−63.

(41) Ferrer, F. J. A.; Improta, R.; Santoro, F.; Barone, V. *Phys. Chem. Chem. Phys.* **2011**, *13*, 17007−17012.

(42) Marcus, R. A. *J. Chem. Phys.* **1963**, *38*, 335.

(43) Tapavicza, E.; Tavernelli, I.; Rothlisberger, U.; Filippi, C.; Casida, M. E. *J. Chem. Phys.* **2008**, *129*, 124108.

(44) Frisch, M. J. et al. *Gaussian 09*, revision A.02; Gaussian Inc.: Wallingford, CT, 2009.

(45) Santoro, F.; Barone, V.; Improta, R. *ChemPhysChem* **2008**, *9*, 2531−2537.

(46) Levine, B. G.; Ko, C.; Quenneville, J.; Martinez, T. J. *Mol. Phys* **2006**, *104*, 1039−1051.

(47) Tapavicza, E.; Tavernelli, I.; Rothlisberger, U. *Phys. Rev. Lett.* **2007**, *98*, 023001.

(48) Haiser, K.; Fingerhut, B. P.; Heil, K.; Glas, A.; Herzog, T. T.; Pilles, B. M.; Schreier, W. J.; Zinth, W.; de Vivie-Riedle, R.; Carell, T. *Angew. Chem., Int. Ed.* **2012**, *51*, 408−411.

(49) Gustavsson, T.; Banyasz, A.; Importa, R.; Markovitsi, D. *J. Phys. Conf. Ser.* **2011**, *261*, 012009.

(50) Blais, J.; Douki, T.; Vigny, P.; Cadet, J. *Photochem. Photobiol.* **1994**, *59*, 402−404.

(51) Markovitsi, D.; Sharonov, A.; Onidas, D.; Gustavsson, T. *ChemPhysChem* **2003**, *3*, 303−305.

(52) Salet, C.; Bensasson, R.; Becker, R. S. *Photochem. Photobiol.* **1979**, *30*, 325−329.

(53) Gut, I. G.; Wood, P. D.; Redmond, R., W. *J. Am. Chem. Soc.* **1996**, *118*, 2366−2373.
(54) Barone, V.; Cossi, M.; Tomasi, J. *J. Chem. Phys.* **1997**, *107*, 3210−3221.
(55) Serrano-Perez, J. J.; Gonzalez-Ramirez, I.; Coto, P. B.; Merchan, M.; Serrano-Andres, L. *J. Phys. Chem. B* **2008**, *112*, 14096−14098.
(56) Gustavsson, T.; Banyasz, A.; Lazzarotto, E.; Markovitsi, D.; Scalmani, G.; Frisch, M. J.; Barone, V.; Improta, R. *J. Am. Chem. Soc.* **2006**, *128*, 607−619.
(57) Santoro, F.; Barone, V.; Gustavsson, T.; Improta, R. *J. Am. Chem. Soc.* **2006**, *128*, 16312−16322.
(58) Barone, V.; Improta, R.; Rega, N. *Acc. Chem. Res.* **2008**, *41*, 605−616.
(59) Biemann, L.; Kovalenko, S. A.; Kleinermanns, K.; Mahrwald, R.; Markert, M.; Improta, R. *J. Am. Chem. Soc.* **2011**, *133*, 19664−19667.
(60) Middleton, C. T.; Cohen, B.; Kohler, B. *J. Phys. Chem. A* **2007**, *111*, 10460−10467. West, B. A.; Womick, J. M.; Moran, A. M. *J. Chem. Phys.* **2011**, *135*, 114505.
(61) Mills, J. B.; Vacano, E.; Hagerman, P. J. *J. Mol. Biol.* **1999**, *285*, 245−257.
(62) Nachtigallova, D.; Hobza, P.; Ritze, H. H. *Phys. Chem. Chem. Phys.* **2008**, *10*, 5689−5697.
(63) Middleton, C. T.; de La Harpe, K.; Su, C.; Law, U. K.; Crespo-Hernández, C. E.; Kohler, B. *Annu. Rev. Phys. Chem.* **2009**, *60*, 217−239.
(64) Stuhldreier, M. C.; Schüler, C.; Kleber, J.; Temps, F. In *Ultrafast Phenomena XVII*; Chergui, M., Jonas, D., Riedle, E., Schoenlein, R. W., Taylor, A., Eds.; Oxford University Press: Cary, NC, 2011; pp 553−555.
(65) Pan, Z. Z.; Hariharan, M.; Arkin, J. D.; Jalolov, A. S.; McCullagh, M.; Schatz, G. C.; Lewis, F. D. *J. Am. Chem. Soc.* **2011**, *133*, 20793−20798.
(66) Improta, R.; Santoro, F.; Barone, V.; Lami, A. *J. Phys. Chem. A* **2009**, *113*, 15346−15354.
(67) Yuan, S.; Zhang, W.; Liu, L.; Dou, Y.; Fang, W.; Lo, G. V. *J. Phys. Chem. A* **2011**, *115*, 13291−13297.
(68) Hare, P. M.; Crespo-Hernández, C.; Kohler, B. *Proc. Natl. Acad. Sci. U.S.A.* **2007**, *104*, 435−440.
(69) Gurzadyan, G. G.; Gorner, H. *Photochem. Photobiol.* **1996**, *63*, 143−153.
(70) *CONICAL INTERSECTIONS Theory, Computation and Experiment*; Domcke, W., Yarkony, Y. R., Köppel, H., Eds.; World Scientific: Singapore, 2011.